Macromolecules

Article

pubs.acs.org/Macromolecules

Relationship between Ion Dissociation, Melt Morphology, and Electrochemical Performance of Lithium and Magnesium Single-Ion Conducting Block Copolymers

Jacob L. Thelen,[†,§,∥] Sebnem Inceoglu,[§,∥] Naveen R. Venkatesan,[†,‡] Nikolaus G. Mackay,[†] and Nitash P. Balsara*[,†,§,∥,⊥]

[†]Department of Chemical and Biomolecular Engineering and [‡]Department of Materials Science and Engineering, University of California, Berkeley, Berkeley, California 94720, United States

[§]Materials Sciences Division, [∥]Joint Center for Energy Storage Research (JCESR), and [⊥]Environmental Energy Technologies Division, Lawrence Berkeley National Laboratory, Berkeley, California 94720, United States

Supporting Information

ABSTRACT: Single-ion conducting block copolymers, such as poly(ethylene oxide)-*b*-poly[(styrene-4-sulfonyltrifluoromethylsulfonyl)imide lithium] (PEO−P[(STFSI)Li]), represent an exciting new class of materials capable of improving the performance of solid-state batteries with metal anodes. In this work, we report on the synthesis and characterization of a matched set of lithiated (PEO−P[(STFSI)Li]) and magnesiated (PEO−P[(STFSI)$_2$Mg]) single-ion conducting diblock copolymers. We measure the temperature dependence of ionic conductivity, and through analysis using the Vogel−Tamman−Fulcher (VTF) relation, demonstrate that ion dissociation is significantly lower for all PEO−P[(STFSI)$_2$Mg] samples when compared to their PEO−P[(STFSI)Li] counterparts. The VTF parameter characterizing the activation barrier to ion hopping was similar for both cations, but the VTF prefactor that reflects effective charge carrier concentration was higher in the lithiated samples by an order of magnitude. We study the melt morphology of the single-ion conducting block copolymers using temperature-dependent X-ray scattering and use the mean-field theory of Leibler to extract the effective Flory−Huggins interaction parameter (χ) for PEO/P[(STFSI)Li] and PEO/P[(STFSI)$_2$Mg] from the X-ray scattering data. We demonstrate a linear relationship between the charge-concentration-related VTF parameter and the parameter quantifying the enthalpic contribution to χ. It is evident that ion dissociation and block copolymer thermodynamics are intimately coupled; ion dissociation in these systems suppresses microphase separation.

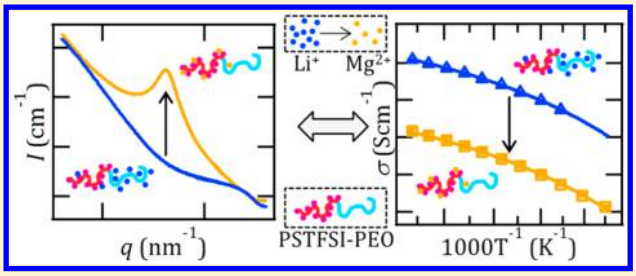

INTRODUCTION

The development of high energy density electrical storage represents an essential task necessary for the efficient implementation of renewable energy sources toward portable technologies, transportation, and improvements to the electrical grid.[1−3] High energy density batteries represent one solution to portable or grid storage; however, to achieve the energy capacities required for demanding applications such as electric vehicles, next-generation batteries will almost certainly require the use of a metal foil anode.[4,5] The use of metal foils, such as lithium, as anodes in rechargeable battery cells introduces many complications, including chemical instability with liquid electrolytes and uneven metal deposition that can lead to a short circuit.[6] One successful approach to mitigating these effects and producing a safe lithium foil battery is to utilize a solid polymer electrolyte.[7]

Most research into the development of solid polymer electrolytes has centered around systems utilizing salt-doped poly(ethylene oxide) (PEO), which is known to readily solvate and conduct ions.[8] Recently a new class of polymer electrolytes has been developed, wherein a block copolymer has an ion-containing block (i.e., the anion is covalently bonded the polymer backbone) and a neutral block, such as PEO, that can solvate and transport the counterions from the ion-containing block.[9] As demonstrated by Bouchet and co-workers, triblock copolymers of poly(ethylene oxide) (PEO) and the lithiated ion-containing polymer, poly(styrene-4-sulfonyltrifluoromethylsulfonyl)imide lithium P[(STFSI)Li], behave as efficient single-ion (i.e., Li$^+$) conductors that can significantly improve the performance of lithium metal batteries.[10]

In addition to the development of lithium metal batteries, there is significant interest in the development of alternative metal foil battery chemistries, such as magnesium metal, which could provide similar energy density, while decreasing both raw material cost and the hazards associated with pyrophoric nature of lithium.[11] Unfortunately, stable magnesium conducting

Received: August 29, 2016
Revised: November 3, 2016
Published: November 17, 2016

DOI: 10.1021/acs.macromol.6b01886
Macromolecules 2016, 49, 9139−9147

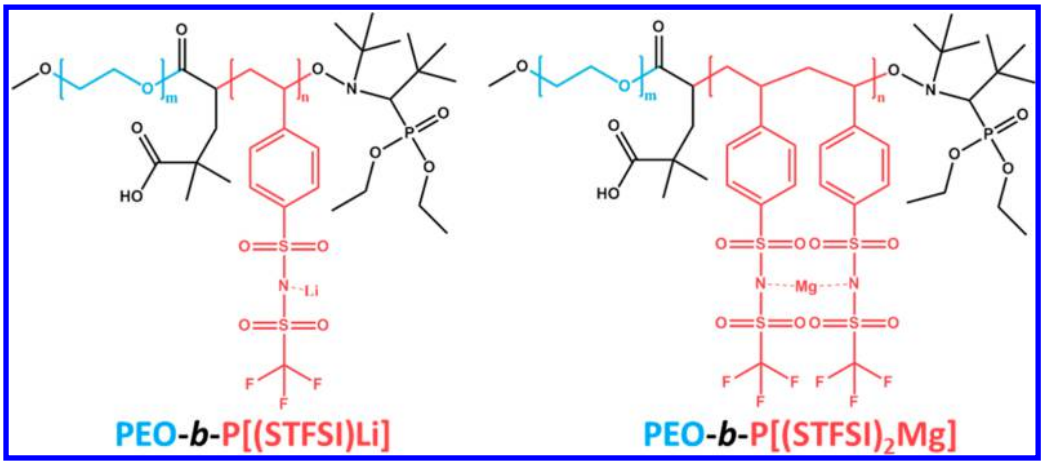

Figure 1. Chemical structure for both types of single-ion block copolymers characterized in this study (including end groups).

Table 1. Characteristics of the Matched Set of Block Copolymers[a]

sample name	$M_{n,PEO}$ (kg mol^{-1})	$M_{n,PSTFSI}$ (kg mol^{-1})	N_{PEO}	N_{PSTFSI}	ϕ_{PSTFSI}	r ([cation][EO]$^{-1}$)
PEO−P[(STFSI)Li](5-3.2)	5.00	3.19	114	9.9	0.32	0.087
PEO−P[(STFSI)Li](5-2.0)	5.00	1.99	114	6.2	0.24	0.054
PE0−P[(STFSI)Li](5-1.1)	5.00	1.05	114	3.3	0.16	0.029
PEO−P[(STFSI)$_2$Mg](5-3.2)	5.00	3.24	114	9.9	0.33	0.043
PEO−P[(STFSI)$_2$Mg](5-2.0)	5.00	2.02	114	6.2	0.24	0.027
PEO−P[(STFSI)$_2$Mg](5-1.1)	5.00	1.08	114	3.3	0.16	0.014
PEO(5)	5.00		114			

[a] $M_{n,PEO}$ and $M_{n,PSTFSI}$ are the number-average molecular weights of each block, with corresponding number-average degrees of polymerization N_{PEO} and N_{PSTFSI}. ϕ_{PSTFSI} is the volume fraction of the ion-containing block, and r is the ratio of cations to ethylene oxide (EO) moieties in each sample.

electrolytes have yet to be developed.[11−15] We demonstrate the development of magnesium-based single-ion conducting block copolymers.

This study is based on a matched-set of lithiated (Li^+) and magnesiated (Mg^{2+}) single-ion conducting PEO−P(STFSI) block copolymers with varying P(STFSI) block length (i.e., charge concentration). We first explore the impact of counterion (Li^+ vs Mg^{2+}) on the ionic conductivity using temperature-dependent potentiostatic electrochemical impedance spectroscopy (PEIS). Our analysis reveals that the number of effective charge carriers contributing to the conductivity for the lithiated sample is about an order of magnitude higher than its magnesiated counterpart. To probe the nanoscale morphology of the single-ion conducting block copolymers, we performed temperature-dependent small- and wide-angle X-ray scattering (SAXS/WAXS) measurements. Our analysis reveals that counterion dissociation in single-ion conducting block copolymers of PEO−P(STFSI) induces compatibility between the two blocks, which in the case of PEO−P[(STFSI)Li] leads to negative effective Flory−Huggins interaction parameters (χ). In conventional block copolymers, thermodynamically driven self-assembly through microphase separation is often leveraged to improve bulk mechanical properties of the electrolyte film.[16−20] The results presented in this paper suggest that this approach is not applicable to single-ion conducting block copolymer electrolytes; single-ion systems with efficient ion conduction are unlikely to exhibit microphase separation. In this scenario, a new strategy must be employed to provide the mechanical support necessary to suppress uneven metal deposition in metal foil batteries,[16,20,21] for example, the introduction of a third incompatible rigid block, such as polystyrene.

EXPERIMENTAL SECTION

Polymer Synthesis and Characterization. PEO−P(STFSI) polymers with a constant PEO molecular weight and varying P(STFSI) block length were synthesized as described previously.[22,23] The synthesis of block copolymers was confirmed through gel permeation chromatography (see SI 1), and the molecular weights of the P(STFSI) blocks were determined through ^{1}H NMR spectroscopy (see SI 2). The polymerization product has potassium counterions for the ion-containing block, which were exchanged through dialysis with lithium chloride (LiCl), as described previously,[22,23] and magnesium chloride ($MgCl_2$) in deionized water to form PEO−P[(STFSI)Li] and PEO−P[(STFSI)$_2$Mg], respectively. The success of the magnesium ion exchange was confirmed through Instrumental Neutron Activation Analysis (INAA) of Cl, F, Mg, and K on PEO-P[(STFSI)$_2$Mg] samples (Elemental Analysis Inc., see SI 3 for details). The chemical structures of each type of the single-ion conducting block copolymer are shown in Figure 1. All of the polymers studied in this work are listed in Table 1. The PEO−P[(STFSI)Li] and PEO−P[(STFSI)$_2$Mg] samples were subsequently dried under vacuum for a minimum of 1 week at ambient temperature and then dried under vacuum in a heated glovebox antechamber at 90 °C for 24 h before being brought into an argon (Ar) glovebox (MBraun). An inert atmosphere was maintained for all subsequent sample preparation and analysis.

Thermal transitions in PEO, PEO−P[(STFSI)Li], and PEO−P[(STFSI)$_2$Mg] were probed using differential scanning calorimetry (DSC). Samples were prepared in an Ar glovebox by placing 6−8 mg of polymer into a TZero aluminum pan and sealing with a TZero hermetic lid (T.A. Inc.). A reference TZero hermetically sealed pan was also prepared in the Ar glovebox. The actual mass of polymer in the pans was recorded as the difference in mass of the pan and lid before and after polymer addition. In order to ensure the polymers had consistent thermal history, the hermetically sealed DSC samples (and reference pan) were subsequently annealed at 135 °C in a vacuum oven at −10 mmHg for 24 h, after which the heater was turned off and the samples were allowed to slowly cool. Measurements were

DOI: 10.1021/acs.macromol.6b01886
Macromolecules 2016, 49, 9139−9147

performed a minimum of 72 h after the oven heater was turned off. A heat−quench−heat−cool method was used in order to determine the PEO melting temperature ($T_{m,PEO}$), crystallization temperature ($T_{c,PEO}$), and, in cases where observable, glass transition temperature ($T_{g,PEO}$). Details of the DSC method used and analysis performed can be found in the Supporting Information (SI 4).

Electrochemical Characterization. The electrochemical response of the ion-containing block copolymers was monitored using potentiostatic electrochemical impedance spectroscopy (PEIS) on symmetric two-electrode cells. The samples used for PEIS were prepared by melting polymer into a 1/8 in. inner diameter spacer made of 10 mil thick silicone elastomer placed upon a stainless steel shim electrode. After filling the spacer with polymer, a second stainless steel shim was placed on top to seal the polymer within the spacer and serve as the counter electrode. Aluminum tabs were used to contact the stainless steel electrodes, and the entire assembly was vacuum sealed in an air-free pouch material (Showa Denko). The samples were subsequently removed from the Ar glovebox and mounted to a custom-built heating stage for variable-temperature electrochemical analysis. Triplicate samples of each ion-containing block copolymer were prepared.

PEIS measurements were performed using a Biologic VMP3 multichannel potentiostat utilizing a 50 mV excitation voltage over a frequency range of 1 MHz−0.5 Hz. The measurements were performed during a cooling temperature scan, where the samples were first heated to 130 °C and held at temperature for 3 h before cooling in 10 °C intervals down to 30 °C. The samples were equilibrated for 1 h at each temperature before performing PEIS measurements.

Resistance due to ion motion was interpreted as the real impedance of the low frequency minimum on a Nyquist plot. In cases of extremely resistive semicrystalline samples, the real impedance at 60 Hz was used to approximate the resistance due to ion motion. The ionic conductivity (σ) was calculated from the real impedance measurements and the sample geometry by $\sigma = L/A_s Z_{Re}$, where L is the sample thickness, A_s is the area defined by the silicone spacer, and Z_{Re} is the real contribution to the impedance measured through PEIS. The reported conductivity values represent the average of the three replicate samples, with error bars that represent their standard deviation from the mean.

Small- and Wide-Angle X-ray Scattering (SAXS/WAXS). X-ray scattering samples were prepared by melt-forming the polymer samples into a 1/8 in. diameter spacer made of 1/32 in. thick Aflas rubber. The polymer/spacer assembly was subsequently covered with 1 mil Kapton film windows and enclosed in a custom-built hermetically sealing aluminum sample holder. The hermetically sealed samples, as well as the empty reference sample, were then removed from the Ar glovebox and annealed in a vacuum oven following the same thermal treatment as the DSC samples. SAXS/WAXS experiments were performed at Lawrence Berkeley National Laboratory's Advanced Light Source, Beamline 7.3.3.[24] Measurements were performed in transmission geometry using a custom-built heated sample stage and the Pilatus 2M detector (see SI 7). Each experiment was replicated using both a SAXS setup with a sample-to-detector (S−D) distance of approximately 3.8 m through an evacuated flight tube and a WAXS configuration utilizing a S−D distance of ∼0.3 m through ambient air. The exact S−D distance for each experiment was determined using a silver behenate (AgB) calibration standard. For each experiment, the stage temperature was set directly to 130 °C and held at that temperature for at least 1 h. The stage was subsequently cooled in either 10 or 20 °C steps down to 90 °C, equilibrating at least 30 min at each temperature before the scattering patterns were measured. The sample temperature at each step was determined by the reading of a dummy sample with an inserted thermocouple (details in SI 5). On average, the sample temperature was found to be a factor of 0.94 times the stage set point temperature. For simplicity, we refer to the stage set point temperature throughout the text; however, all analysis accounts for the temperature offset.

The scatting data were reduced using the Nika macro developed by Jan Ilavsky[25] in Igor Pro. The beam center and S−D distance were calibrated using the scattering from the AgB standard, and an image mask was used to exclude dead pixels and shadows from the beamstop. The isotropic 2D scattering patterns were azimuthally averaged to yield 1D data sets of intensity (I) versus the magnitude of the scattering vector (q), where $q = (4\pi/\lambda)\sin(\theta/2)$, λ is the X-ray wavelength, and θ is the scattering angle. The averaged SAXS and WAXS intensities were further corrected for sample transmission, parasitic scattering from the sample holder, and then calibrated to absolute units (cm^{-1}) using a glassy carbon intensity standard provided by Jan Ilavsky (Sample M13).[26] Details of the data corrections can be found in the Supporting Information (SI 7). Independent calibration of the SAXS and WAXS intensities allows for the I versus q scattering profiles to be combined without arbitrary scaling, providing structural information over a wide range of length scales, i.e., $0.04 < q < 35$ nm^{-1}, which in real space probes length scales from ∼150 nm down to ∼0.2 nm. For the purposes of this study, we limit our analysis to structures on the order the polymer chain dimensions and focus on $0.04 < q < 4$ nm^{-1}; however, a detailed treatment of the WAXS scattering ($q > 4$ nm^{-1}) and semicrystalline structures in these single-ion block copolymers will be the focus of a forthcoming study.

RESULTS AND DISCUSSION

The results of the DSC analysis for all of the samples are summarized in Table 2. All samples exhibited PEO melting peaks after the thermal pretreatment described in the Experimental Section; however, crystallization during the cooling scan was significantly depressed for PEO−P[(STFSI)$_2$Mg](5-3.2) and was not observed in the PEO−P[(STFSI)Li](5-3.2) sample. The inhibited crystallization in these samples facilitated the observation of the glass transition of PEO (T_g), whereas the strong crystallization of PEO in the other samples precluded the observation of a T_g.

Table 2. Sample Details and Results from DSC Analysis[a]

sample name	sample mass (mg)	$T_{m,PEO}$ (°C)	$T_{c,PEO}$ (°C)	$T_{g,PEO}$ (°C)
PEO−P[(STFSI)Li](5-3.2)	8.0	55.7	–	−34
PEO−P[(STFSI)Li](5-2.0)	7.1	57.9	35.7	–
PEO−P[(STFSI)Li](5-1.1)	7.0	58.1	35.3	–
PEO−P[(STFSI)$_2$Mg](5-3.2)	8.1	57.2	−28.5	−39
PEO−P[(STFSI)$_2$Mg](5-2.0)	6.4	57.2	17.2	–
PEO−P[(STFSI)$_2$Mg](5-1.1)	7.2	57.9	23.9	–
PEO(5)	6.5	59.8	42.2	–

[a]A dash (−) indicates that the transition was not observed.

The results of the variable-temperature PEIS analysis of the PEO−P[(STFSI)Li] and PEO−P[(STFSI)$_2$Mg] single-ion conducting block copolymers are shown in Figure 2a, where ionic conductivity is plotted in Arrhenius fashion versus reciprocal temperature. Qualitatively, at temperatures above the melting point of PEO, all of the samples exhibit the modified Arrhenius (i.e., Vogel−Tamman−Fulcher, VTF) behavior typical of polymer electrolytes, wherein ion motion is linked to the dynamics of the solvating polymer chains.[8] At temperatures below the melting point of PEO, the crystallization of the PEO chains freezes the dynamics of most samples and causes a precipitous drop in ionic conductivity down to the limits of instrumental noise for the potentiostat. For clarity, we omit the conductivity values from samples that have crystallized; however, the data from all temperatures can be found in Figure S7 of the Supporting Information.

The first major takeaway from the conductivity data is that for all molecular weights, the lithiated samples exhibit ionic

DOI: 10.1021/acs.macromol.6b01886
Macromolecules 2016, 49, 9139−9147

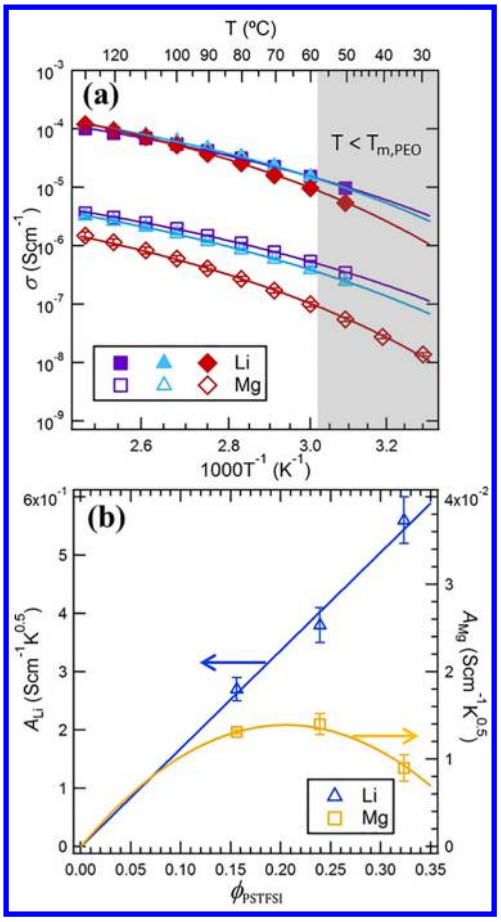

Figure 2. (a) Measured temperature-dependent ionic conductivity for all single-ion conducting block copolymer samples. Closed symbols correspond to Li^+, and open symbols correspond to Mg^{2+} with purple squares = PEO−P(STFSI)(5-1.1), cyan triangles = PEO−P(STFSI)-(5-2.0), and red diamonds = PEO−P(STFSI)(5-3.2). Solid curves represent the nonlinear least-squares fits to the VTF equation. The shaded region denotes temperatures below the melting point of PEO where crystallization is expected to occur. (b) The VTF fit coefficient A, reflecting the number of effective charge carriers per volume, plotted as a function of the volume fraction of ion-containing block for both the lithiated and magnesiated polymers. Error bars represent the uncertainty in the value for A from the least-squares regression of the VTF fitting, and solid line/curve represent the least-squares best fits to the data: $A_{Li} = 1.68\phi_{PSTFSI}$ and $A_{Mg} = 0.136\phi_{PSTFSI} - 0.33\phi_{PSTFSI}^2$.

conductivities about an order of magnitude higher than their magnesiated counterparts. In principle, the differences in conductivity could be due to either a difference in the energetic barrier to ion motion (e.g., activation energy) or in the amount of effective charge carriers within the sample. To differentiate between these two potential causes, we fit the temperature-dependent data to the well-known VTF equation[8]

$$\sigma(T) = \frac{A}{\sqrt{T}} e^{-B/R[T-(T_g-50)]} \quad (1)$$

where A and B are fitting parameters relating the effective charge carrier concentration and pseudoactivation energy, respectively, and T_g is the glass transition temperature of the conducting polymer phase. As noted previously, only PEO−P[(STFSI)Li](5-3.2) and PEO−P[$(STFSI)_2$Mg](5-3.2) exhibited T_g's in DSC. Therefore, the conductivity of the PEO−P[(STFSI)Li](5-3.2) and PEO−P[$(STFSI)_2$Mg](5-3.2) samples were fit with the VTF equation using A and B as adjustable parameters and the measured $T_{g,PEO}$ from DSC analysis (Table 2). To limit the number of adjustable parameters in our fits, B was held constant for the rest of the lithiated and magnesiated series (B_{Li} = 9.6 ± 0.1 kJ/mol and B_{Mg} = 10.5 ± 0.2 kJ/mol). By using a constant value for B, we assume that the activation barrier to ion hopping does not change significantly with ion concentration in our samples, but rather the apparent activation barrier for ion conduction is only attenuated by differences in polymer dynamics (i.e., the T_g of the conducting phase). All fit parameters with their respective uncertainties are listed in Table S3. We note that value of B determined for the lithiated and magnesiated versions of PEO−P(STFSI)(5-3.2) are similar, within 10%, and within the range typically observed for PEO-based polymer electrolytes with added salt.[27,28] The major cause of the difference in conductivity values observed for the PEO−P[(STFSI)Li] and PEO−P[$(STFSI)_2$Mg] is highlighted in Figure 2b, where A from VTF analysis is plotted versus the volume fraction of ion-containing block, ϕ_{PSTFSI}. In the case of the lithiated polymers, A_{Li} directly correlates with the total concentration of charge, as demonstrated by the linear fit through the origin in Figure 2b. The magnesiated polymers, however, have a more complex relationship between A_{Mg} and ϕ_{PSTFSI}, which we found to be best described by the quadratic fit through the origin shown in Figure 2b. Perhaps more importantly, comparing of the absolute values of A_{Li} and A_{Mg} reveals that in all cases A_{Mg} is more than an order of magnitude lower than A_{Li}. Since it is generally believed that the VTF parameter A reflects the concentration of effective charge carriers,[8] we conclude that the concentration of free magnesium ions in the PEO−P-[$(STFSI)_2$Mg] samples is approximately an order of magnitude smaller than that of free lithium in the PEO−P[(STFSI)Li] samples. This behavior is consistent with the nature of the charged species; one expects less dissociation in systems with divalent cations such as Mg^{2+} when compared to monovalent cations such as Li^+. We note that further work is needed to establish the efficacy of Mg^{2+} transport in our polymers. For example, in addition to less dissociation, one may also expect a decrease is mobility of divalent cations due to their ability to bind two different polymer chains, thereby creating physical cross-links. Furthermore, it is important to measure steady-state currents in symmetric Mg−polymer−Mg cells to ascertain that our electrolyte is a single-ion conductor. We note that such experiments are much more difficult than the analogous experiments on lithiated polymers[10,22,23] due to difficulties in reversible stripping and plating of magnesium.[13,29,30]

While there is considerable data on conductivity of lithium single-ion conductors,[10,22,23,31] to our knowledge, there are no studies reporting conductivity values for magnesium single-ion conductors. Most work in the development of Mg^{2+} electrolytes has focused on liquid systems,[13,30,32] and many of the studies on polymer electrolytes have used divalent salts that do not solvate as readily as those composed of the bis(trifluoromethanesulfonyl)imide (TFSI) anion (e.g., $Mg(TFSI)_2$).[33−35] The work of Lee and Allcock,[36] wherein they directly compare the conductivities of electrolytes prepared from LiTFSI and $Mg(TFSI)_2$ with the same polymer, poly[bis(2-(2-methoxyethoxy)ethoxy)phosphazene] (MEEP), seems most relevant to this work. They observed similar conductivities between MEEP/LiTFSI and MEEP/$Mg(TFSI)_2$ samples; thus, electrolytes composed of divalent cations do not have intrinsically lower conductivities than those composed of monovalent

DOI: 10.1021/acs.macromol.6b01886
Macromolecules 2016, 49, 9139−9147

cations. Lee and Allcock hypothesized that the measured conductivities were due predominantly to anion motion, although they did not attempt to measure steady-state currents to prove that conjecture. In our case, anion motion is precluded; thus, we attribute our observed conductivity values to the motion of Li^+ and Mg^{2+}. We have not found any evidence that the motion of Mg^{2+} is intrinsically limited in this new class of single-ion conducting block copolymers.

Figure 3 shows the X-ray scattering profiles of both sets of polymers in absolute units, with the absolute scattering

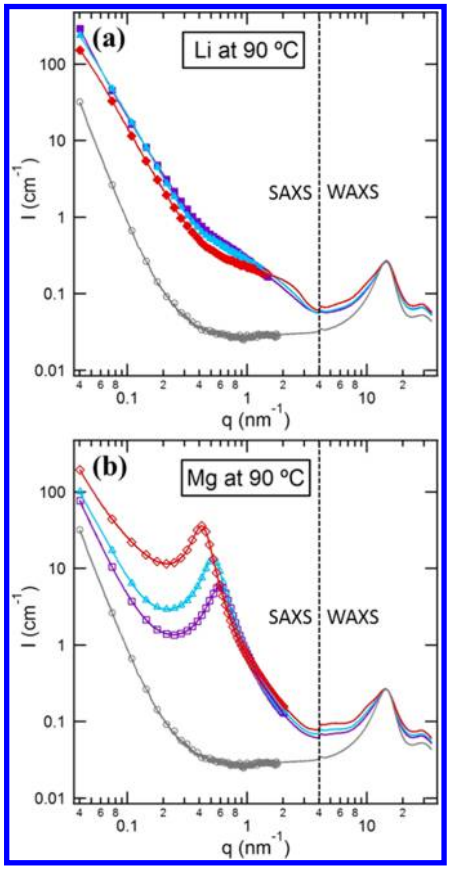

Figure 3. Combined SAXS/WAXS profiles for (a) PEO−P[(STFSI)-Li] (closed symbols) and (b) PEO−P[(STFSI)$_2$Mg] (open symbols) samples after cooling from 130 °C down to 90 °C; scattering intensity, I, is plotted versus the magnitude of the scattering vector, q. Purple squares/curves = PEO−P(STFSI)(5-1.1), cyan triangles/curves = PEO−P(STFSI)(5-2.0), and red diamonds/curves = PEO−P(STFSI)-(5-3.2). For clarity, SAXS data markers are only plotted for every 15th data point and WAXS data are represented by lines only. Scattering from PEO(5) is shown for reference (open gray circles/curves) on both plots. All intensities are presented on an absolute scale. The dashed vertical lines indicate our demarcation between the SAXS and WAXS scattering regimes, which we chose based on the intensity upturn from the first amorphous WAXS halo. The feature in the scattering data near q = 4 nm^{-1} is due to imperfect subtraction of the scattering from the Kapton sample holder windows.

intensity of PEO(5) for reference at 90 °C (in the melt state). These profiles were obtained by combining the SAXS and WAXS data as described in the Experimental Section. The lack of scattering peaks in the SAXS profiles for PEO−P[(STFSI)Li] in Figure 5a is consistent with previous observations.[22,23] The SAXS profile of PEO−P[(STFSI)Li](5-3.2) contains a weak shoulder in the vicinity of q = 2.5 nm^{-1}. This may be due to the so-called ionomer peak,[37] reflecting the presence of ionic domains with an average interdomain spacing of ∼2.5 nm. Determining the nature of these domains is beyond the scope of the present study. The SAXS profiles for PEO−P[(STFSI)$_2$Mg], on the other hand, contain a broad primary scattering peak. The lack of higher order peaks suggests that the primary scattering peak reflects disordered concentration fluctuations.[38] The position of the primary peak shifts to lower q-values as the P[(STFSI)$_2$Mg] block length increases, consistent with the theory of Leibler.[38]

Theoretical predictions for scattering profiles from ion-containing block copolymers have not yet been proposed. Lacking a better alternative, we use the mean-field theory of uncharged block copolymers proposed by Leibler[38] to analyze our scattering profiles. In Figure 4 we show least-squares fits of the well-known Leibler structure factor[38,39] modified to account for polymer chain length dispersity[40] for the magnesiated block copolymers. The fitted parameters for the magnesiated samples are the overall polymer radius of gyration (R_g), which is determined by the position of the scattering peak, and the Flory−Huggins interaction parameter (χ) between PEO and P(STFSI). Detailed information regarding the fitting procedure is provided in the Supporting Information (SI 8). As demonstrated in Figure 4, the Leibler structure factor provides a reasonable fit to the PEO−P[(STFSI)$_2$Mg] scattering. The excess scattering intensity for low q-values seen in the magnesiated block copolymer data in Figure 4 is similar to that observed in other ion-containing block copolymers.[9,28,41] Encouraged by the results from PEO−P[(STFSI)$_2$Mg], we also attempted to model the scattering from the PEO−P[(STFSI)-Li]. The radius of gyration of the lithiated samples could not be determined from X-ray scattering due to the lack of a scattering peak. Lacking a better alternative, we used the radius of gyration (R_g) values determined from the matched PEO−P[(STFSI)$_2$Mg] sample for each lithiated sample. Thus, the only adjustable parameter for the Leibler structure factor of the PEO−P[(STFSI)Li] samples was the Flory−Huggins interaction parameter (χ). The χ parameters reported here are based on a reference volume of 0.1 nm^3. All parameters obtained from the fits described here are given in Tables S4−S6 in the Supporting Information.

The dependence of the Flory−Huggins interaction parameter on ϕ_{PSTFSI} for both lithiated and magnesiated block copolymers at 90 °C is shown in Figure 4d. In the case of magnesiated copolymers, χ is positive and decreases with increasing ϕ_{PSTFSI}. In contrast, χ values obtained from PEO−P[(STFSI)Li](5-2.0) and PEO−P[(STFSI)Li](5-3.2) are negative; i.e., no positive value of χ could suitably model the scattering from the PEO−P[(STFSI)Li](5-2.0) and PEO−P[(STFSI)Li](5-3.2) samples. The black dashed curves in Figures 4a−c indicate the predicted scattering for χ = 0. The only lithiated sample with a positive χ is PEO−P[(STFSI)Li]-(5-1.1).

The fitting procedure described above was applied to data obtained at 110 and 130 °C to determine the temperature dependence of χ_{Li} and χ_{Mg}. Figure 5a shows the result of this analysis in a plot of χ versus inverse temperature. The solid lines through each data set represent the linear least-squares fit to eq 2

$$\chi(T) = \alpha + \frac{\beta}{T} \quad (2)$$

DOI: 10.1021/acs.macromol.6b01886
Macromolecules 2016, 49, 9139−9147

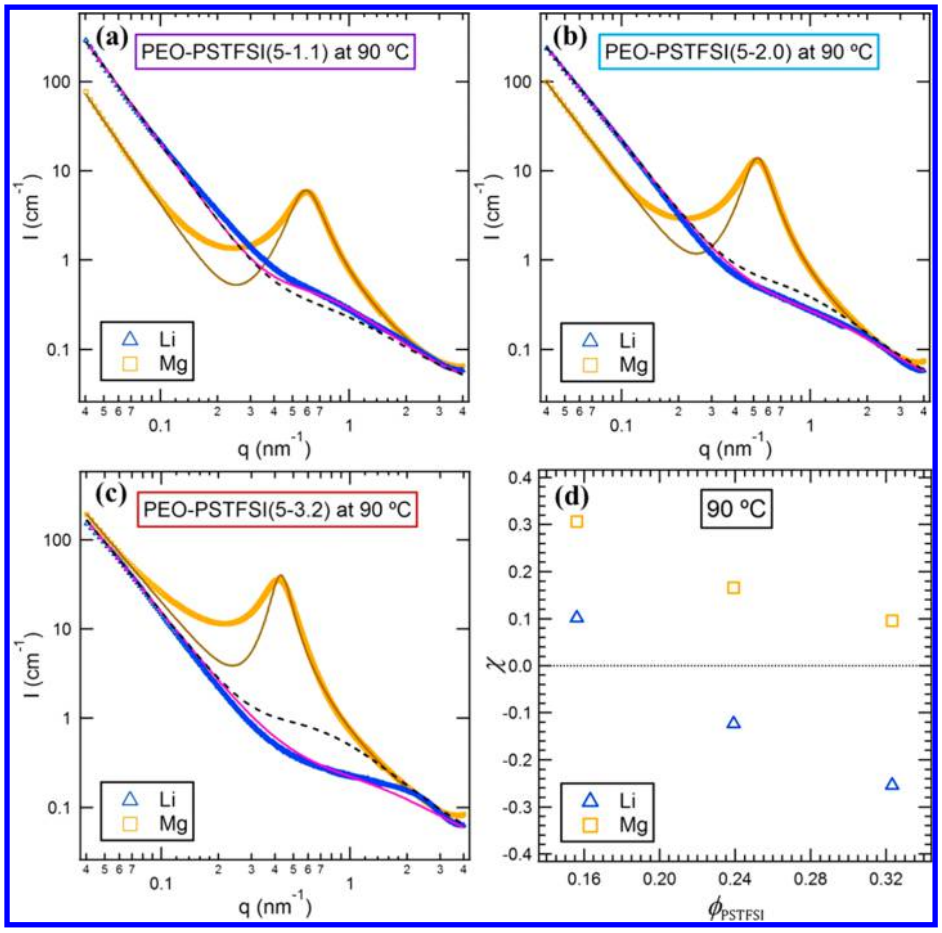

Figure 4. (a–c) Scattering intensity, I, versus magnitude of the scattering vector, q, of lithiated and magnesiated pairs at 90 °C. Experimental data were fit to Leibler's mean field theory to estimate the Flory–Huggins interaction parameter, χ. Experimental data: lithiated samples = blue triangles; magnesiated samples = gold squares (symbols overlap due to high resolution). Theoretical fits: lithiated samples = solid magenta curves; magnesiated sample = solid dark gold curves. The dashed black curves indicate the model prediction for $\chi = 0$. (d) The fitted χ-parameter values used to model the data in (a–c) versus the volume fraction of ion-containing polymer block, ϕ_{PSTFSI}. Values for PEO–P[(STFSI)Li] samples (χ_{Li}) are indicated by blue triangles, and those for PEO–P[(STFSI)$_2$Mg] (χ_{Mg}) are denoted by gold squares. The $\chi = 0$ axis value is denoted by a dashed line for reference.

where α and β are the fit parameters. In Figure 5b, we plot α versus ϕ_{PSTFSI} for both PEO–P[(STFSI)Li] (α_{Li}) and PEO–P[(STFSI)$_2$Mg] (α_{Mg}) samples. α_{Li} and α_{Mg} have qualitatively opposite trends: α_{Li} increases with increasing ϕ_{PSTFSI} while α_{Mg} decreases with increasing ϕ_{PSTFSI}. In Figure 5c, we plot β versus ϕ_{PSTFSI} for both sets of PEO–P[(STFSI)Li] (β_{Li}) and PEO–P[(STFSI)$_2$Mg] (β_{Mg}) samples. β_{Li} is negative and decreases with increasing ϕ_{PSTFSI}. In contrast, the β_{Mg} values are negligibly small and essentially independent of ϕ_{PSTFSI}.

In Figure 6, we plot β obtained from analysis of the SAXS data versus A obtained from analysis of the PEIS data. It is evident that β and A are correlated, suggesting a relationship between ion dissociation and self-assembly. In the case of PEO–P[(STFSI)$_2$Mg] samples where little ion dissociation occurs, the polymer morphology resembles that of a typical disordered diblock copolymer, with concentration fluctuations on length scales on the order of the radius of gyration of the polymer chains. In the case of PEO–P[(STFSI)Li], on the other hand, dissociation of the lithium ions suppresses concentration fluctuations. Figure 6 provides evidence for the fact that dissociated lithium ions induce mixing of PEO and P(STFSI)Li blocks due to favorable interactions between the ions and PEO.

CONCLUSION

In the pursuit of developing high-energy-density batteries with metallic anodes, single-ion conducting block copolymers represent an exciting class of materials that has demonstrated improvements in battery performance.[10] In this work, we report on the synthesis of a matched set of lithiated and magnesiated single-ion conducting block copolymers, PEO–P[(STFSI)Li] and PEO–P[(STFSI)$_2$Mg]. The melt morphology of the block copolymers was studied by X-ray scattering, and the temperature-dependence of ionic conductivity was determined by PEIS experiments. The effective Flory–Huggins interaction parameter (χ) for PEO/P[(STFSI)Li] and PEO/P-[(STFSI)$_2$Mg] was estimated by analyzing the X-ray scattering data using the mean-field theory of Leibler. The VTF equation was used to analyze the conductivity data. We demonstrate a linear relationship between the parameter β that characterizes the temperature dependence of χ and the VTF parameter A, which reflects the concentration of effective charge carriers. We thus demonstrate that block copolymer polymer self-assembly is coupled to ion dissociation.

There is great interest in using microphase-separated block copolymers as electrolytes due to their ability to decouple electrical and mechanical properties.[16,20] In these systems, the microphase separation is driven by thermodynamic incompat-

DOI: 10.1021/acs.macromol.6b01886
Macromolecules 2016, 49, 9139–9147

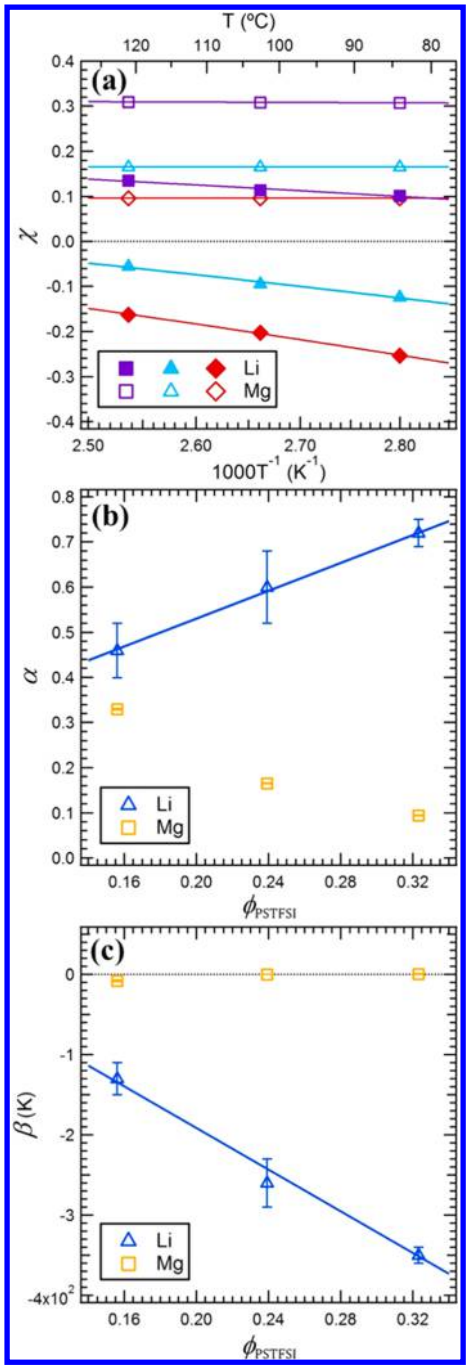

Figure 5. (a) Flory–Huggins interaction parameter, χ, determined by fitting SAXS data versus reciprocal temperature. Closed symbols correspond to Li samples, and open symbols correspond to Mg samples, with purple squares = PEO–P(STFSI)(5-1.1), cyan triangles = PEO–P(STFSI)(5-2.0), and red diamonds = PEO–P(STFSI)(5-3.2). Solid lines indicate the linear least-squares fits to eq 2. The dotted line indicates $\chi = 0$. (b) The fitting constant (α) from eq 2 determined from the linear fits in (a) plotted versus volume fraction of the ion-containing block, ϕ_{PSTFSI}. Values for PEO–P[(STFSI)Li] samples (α_{Li}) are indicated by blue triangles, and those for PEO–P[$(STFSI)_2$Mg] (α_{Mg}) are denoted by gold squares. (c) The fitting constant (β) from eq 2 determined from the linear fits in (a) plotted versus ϕ_{PSTFSI}. Values for PEO–P[(STFSI)Li] samples (β_{Li}) are indicated by blue triangles, and those for PEO–P[$(STFSI)_2$Mg] (β_{Mg}) are denoted by gold squares. Error bars in (b, c) represent the fitting error in the parameters, and solid lines through the α_{Li} and β_{Li} data indicate the linear least-squares fits: $\alpha_{Li} = 0.2 + 1.5\phi_{PSTFSI}$ and $\beta_{Li} = 70 - 1.3 \times 10^3\phi_{PSTFSI}$. The dotted line in (c) indicates $\beta = 0$.

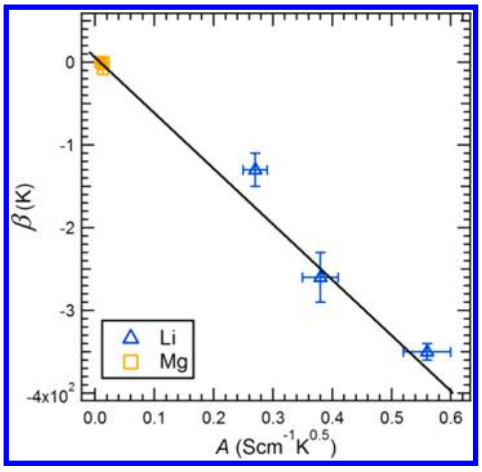

Figure 6. Parameter β, which quantifies the temperature dependence χ ($\chi(T) = \alpha + \beta/T$), plotted as a function of the VTF parameter related to the effective charge carrier concentration (A) for all samples. Error bars represent the fitting uncertainty for each parameter, and the solid line is the best fit to the data accounting for the errors in both axes: $\beta = -670A + 5.9$.

ibility between the polymer blocks, quantified by the product χN. For example, in the case of symmetric block copolymers, microphase separation will occur if χN exceeds 10.5.[38] For the copolymers used in this study, microphase separation is predicted to occur if χN exceeds values ranging from 11 to 30, depending on ϕ_{PSTFSI}. While the χ values determined for the magnesiated samples suggest that microphase separation might occur at larger chain lengths (i.e., larger N) than those used in this study, the values of χ determined for lithiated samples are negative in most cases. We thus predict that PEO–P[(STFSI)Li] will be homogeneous (i.e., not microphase separated), regardless of chain length. (Crystallization of the PEO block can lead to microphase separation in these systems,[22,23] but this phenomenon is not of interest in this study because crystalline PEO is essentially nonconducting.) We have shown that microphase separation only occurs in the absence of ion dissociation. Thus, while we may be able to obtain microphase-separated PEO–P[$(STFSI)_2$Mg] samples, the ionic conductivity of these samples is likely to be very low. To obtain mechanically rigid single-ion conducting block copolymers, it will be necessary to synthesize ABC triblock polymers with an additional incompatible C-block to provide mechanical support (e.g., PEO–P[(STFSI)Li]–PS).

■ ASSOCIATED CONTENT

Supporting Information

The Supporting Information is available free of charge on the ACS Publications website at DOI: 10.1021/acs.macromol.6b01886.

(SI 1) Gel permeation chromatography (GPC); (SI 2) ^{1}H nuclear magnetic resonance (^{1}H NMR); (SI 3) instrumental neutron activation analysis (INAA); and (SI 4) differential scanning calorimetry (DSC) analysis of the single-ion conducting block copolymers; (SI 5) provides the relationship between the stage and sample temperatures during the SAXS/WAXS experiments; all ionic conductivity data and VTF fitting parameters are given in (SI 6), and (SI 7) details the SAXS/WAXS data reduction and calibration procedure as well as providing the temperature-dependent SAXS profiles for all samples;

DOI: 10.1021/acs.macromol.6b01886
Macromolecules 2016, 49, 9139–9147

(SI 8) details the model used to fit the SAXS data as well as the procedure used to achieve the fitted curves shown in the main text (PDF)

AUTHOR INFORMATION

Corresponding Author

*E-mail: nbalsara@berkeley.edu (N.P.B.).

ORCID

Jacob L. Thelen: 0000-0003-0026-4404

Author Contributions

J.L.T. and S.I. contributed equally.

Notes

The authors declare no competing financial interest.

ACKNOWLEDGMENTS

This work was supported by the Joint Center for Energy Storage Research, an Energy Innovation Hub funded by the U.S. Department of Energy (DOE), Office of Science, Basic Energy Sciences (BES). Thermal analysis was performed at the Molecular Foundry at Lawrence Berkeley National Laboratory. X-ray scattering experiments were performed at Lawrence Berkeley National Laboratory's Advance Light Source, Beamline 7.3.3. The Molecular Foundry and Beamline 7.3.3 of the Advanced Light Source are supported by the Director of the Office of Science, Office of Basic Energy Sciences, of the U.S. Department of Energy under Contract DE-AC02-05CH11231. We thank Polite Stewart, Chenhui Zhu, and Eric Schaible for their assistance with the setup and operation of Beamline 7.3.3 as well as Hilda Buss for her assistance with the NMR analysis of the single-ion conducting block copolymers.

ABBREVIATIONS

AgB	silver behenate
DSC	differential scanning calorimetry
EO	ethylene oxide
^{1}H NMR	proton nuclear magnetic resonance
INAA	instrumental neutron activation analysis
MEEP	poly[bis(2-(2-methoxyethoxy)ethoxy)-phosphazene]
PEIS	potentiostatic electrochemical impedance spectroscopy
PEO	poly(ethylene oxide)
PEO−P[(STFSI)Li]	poly(ethylene oxide)-*b*-poly[(styrene-4-sulfonyltrifluoromethylsulfonyl)-imide lithium]
PEO−P[(STFSI)$_2$Mg]	poly(ethylene oxide)-*b*-poly[(styrene-4-sulfonyltrifluoromethylsulfonyl)-imide magnesium]
P(STFSI)	poly[(styrene-4-sulfonyltrifluoromethylsulfonyl)imide], unspecified ion
PS	polystyrene
S−D	sample to detector distance
SAXS	small-angle X-ray scattering
TFSI	bis(trifluoromethanesulfonyl)imide
VTF	Vogel−Tamman−Fulcher
WAXS	wide-angle X-ray scattering

Symbols

A	effective charge carrier concentration (from VTF fit), S cm^{-1} K$^{0.5}$
A_s	conductivity sample electrode area, cm^2
B	effective activation barrier (from VTF fit), kJ mol^{-1}
I	scattering intensity, cm^{-1}
L	conductivity sample thickness, cm
$M_{n,PEO}$	number-average molecular weight of PEO block, kg mol^{-1}
$M_{n,PSTFSI}$	number-average molecular weight of P(STFSI) block, kg mol^{-1}
N_{PEO}	number-average degree of polymerization of PEO block, −
N_{PSTFSI}	number-average degree of polymerization of P(STFSI) block, −
q	magnitude of the scattering vector, nm^{-1}
R	gas constant, kJ mol^{-1} K^{-1}
R_g	radius of gyration, nm
T	temperature, K
$T_{c,PEO}$	crystallization temperature of PEO, °C
T_g	glass transition temperature, K
$T_{g,PEO}$	glass transition temperature of PEO, °C
$T_{m,PEO}$	melting temperature of PEO, °C
Z_{Re}	real component of conductivity sample impedance, Ω

Greek Letters

α	temperature-independent contribution to the interaction parameter, −
β	temperature-dependent contribution to the interaction parameter, K
χ	monomer−monomer interaction parameter, −
ϕ_{PSTFSI}	volume fraction of the P(STFSI) block, −
λ	scattering wavelength, nm
θ	scattering angle, rad
σ	ionic conductivity, S cm^{-1}

REFERENCES

(1) Denholm, P.; Ela, E.; Kirby, B.; Milligan, M. Role of Energy Storage with Renewable Electricity Generation; Golden, CO, 2010.

(2) Denholm, P.; Hand, M. Grid Flexibility and Storage Required to Achieve Very High Penetration of Variable Renewable Electricity. *Energy Policy* **2011**, *39*, 1817−1830.

(3) Jacobson, M. Z.; Delucchi, M. A. Providing All Global Energy with Wind, Water, and Solar Power, Part I: Technologies, Energy Resources, Quantities and Areas of Infrastructure, and Materials. *Energy Policy* **2011**, *39*, 1154−1169.

(4) Tarascon, J. M.; Armand, M. Issues and Challenges Facing Rechargeable Lithium Batteries. *Nature* **2001**, *414*, 359−367.

(5) Article, R.. *Li−O2 and Li−S Batteries with High Energy Storage* **2012**, *11*, 19−30.

(6) Aurbach, D. A Short Review of Failure Mechanisms of Lithium Metal and Lithiated Graphite Anodes in Liquid Electrolyte Solutions. *Solid State Ionics* **2002**, *148*, 405−416.

(7) Schaefer, J. L.; Lu, Y.; Moganty, S. S.; Agarwal, P.; Jayaprakash, N.; Archer, L. A. Electrolytes for High-Energy Lithium Batteries. *Appl. Nanosci.* **2012**, *2*, 91−109.

(8) Vincent, C. A.; MacCallum, J. R. *Polymer Electrolyte Reviews*; Elsevier Applied Science: 1987.

(9) Ryu, S.-W.; Trapa, P. E.; Olugebefola, S. C.; Gonzalez-Leon, J. A.; Sadoway, D. R.; Mayes, A. M. Effect of Counter Ion Placement on Conductivity in Single-Ion Conducting Block Copolymer Electrolytes. *J. Electrochem. Soc.* **2005**, *152*, A158.

(10) Bouchet, R.; Maria, S.; Meziane, R.; Aboulaich, A.; Lienafa, L.; Bonnet, J.; Phan, T. N. T.; Bertin, D.; Gigmes, D.; Devaux, D.; et al. Single-Ion BAB Triblock Copolymers as Highly Efficient Electrolytes for Lithium-Metal Batteries. *Nat. Mater.* **2013**, *12*, 452−457.

(11) Saha, P.; Datta, M. K.; Velikokhatnyi, O. I.; Manivannan, A.; Alman, D.; Kumta, P. N. Rechargeable Magnesium Battery: Current Status and Key Challenges for the Future. *Prog. Mater. Sci.* **2014**, *66*, 1−86.

DOI: 10.1021/acs.macromol.6b01886
Macromolecules 2016, 49, 9139−9147

(12) Muldoon, J.; Bucur, C. B.; Oliver, A. G.; Zajicek, J.; Allred, G. D.; Boggess, W. C. Corrosion of Magnesium Electrolytes: Chlorides — the Culprit. *Energy Environ. Sci.* **2013**, *6*, 482.
(13) Mohtadi, R.; Mizuno, F. Magnesium Batteries: Current State of the Art, Issues and Future Perspectives. *Beilstein J. Nanotechnol.* **2014**, *5*, 1291−1311.
(14) Shterenberg, I.; Salama, M.; Gofer, Y.; Levi, E.; Aurbach, D. The Challenge of Developing Rechargeable Magnesium Batteries. *MRS Bull.* **2014**, *39*, 453−460.
(15) Muldoon, J.; Bucur, C. B.; Oliver, A. G.; Sugimoto, T.; Matsui, M.; Kim, H. S.; Allred, G. D.; Zajicek, J.; Kotani, Y. Electrolyte Roadblocks to a Magnesium Rechargeable Battery. *Energy Environ. Sci.* **2012**, *5*, 5941.
(16) Singh, M.; Odusanya, O.; Wilmes, G. M.; Eitouni, H. B.; Gomez, E. D.; Patel, A. J.; Chen, V. L.; Park, M. J.; Fragouli, P.; Iatrou, H.; et al. Effect of Molecular Weight on the Mechanical and Electrical Properties of Block Copolymer Electrolytes. *Macromolecules* **2007**, *40*, 4578−4585.
(17) Panday, A.; Mullin, S. A.; Gomez, E. D.; Wanakule, N. S.; Chen, V. L.; Hexemer, A.; Pople, J.; Balsara, N. P. Effect of Molecular Weight and Salt Concentration on Conductivity of Block Copolymer Electrolytes. *Macromolecules* **2009**, *42*, 4632−4637.
(18) Hallinan, D. T.; Mullin, S. A.; Stone, G. M.; Balsara, N. P. Lithium Metal Stability in Batteries with Block Copolymer Electrolytes. *J. Electrochem. Soc.* **2013**, *160*, A464−A470.
(19) Young, N. P.; Devaux, D.; Khurana, R.; Coates, G. W.; Balsara, N. P. Investigating Polypropylene-Poly(ethylene Oxide)-Polypropylene Triblock Copolymers as Solid Polymer Electrolytes for Lithium Batteries. *Solid State Ionics* **2014**, *263*, 87−94.
(20) Schauser, N. S.; Harry, K. J.; Parkinson, D. Y.; Watanabe, H.; Balsara, N. P. Lithium Dendrite Growth in Glassy and Rubbery Nanostructured Block Copolymer Electrolytes. *J. Electrochem. Soc.* **2015**, *162*, A398−A405.
(21) Monroe, C.; Newman, J. The Impact of Elastic Deformation on Deposition Kinetics at Lithium/Polymer Interfaces. *J. Electrochem. Soc.* **2005**, *152*, A396.
(22) Inceoglu, S.; Rojas, A. A.; Devaux, D.; Chen, X. C.; Stone, G. M.; Balsara, N. P. Morphology−Conductivity Relationship of Single-Ion-Conducting Block Copolymer Electrolytes for Lithium Batteries. *ACS Macro Lett.* **2014**, *3*, 510−514.
(23) Rojas, A. A.; Inceoglu, S.; Mackay, N. G.; Thelen, J. L.; Devaux, D.; Stone, G. M.; Balsara, N. P. Effect of Lithium-Ion Concentration on Morphology and Ion Transport in Single-Ion-Conducting Block Copolymer Electrolytes. *Macromolecules* **2015**, *48*, 6589−6595.
(24) Hexemer, A.; Bras, W.; Glossinger, J.; Schaible, E.; Gann, E.; Kirian, R.; MacDowell, A.; Church, M.; Rude, B.; Padmore, H. A SAXS/WAXS/GISAXS Beamline with Multilayer Monochromator. *J. Phys.: Conf. Ser.* **2010**, *247*, 012007.
(25) Ilavsky, J. Nika: Software for Two-Dimensional Data Reduction. *J. Appl. Crystallogr.* **2012**, *45*, 324−328.
(26) Zhang, F.; Ilavsky, J.; Long, G. G.; Quintana, J. P. G.; Allen, A. J.; Jemian, P. R. Glassy Carbon as an Absolute Intensity Calibration Standard for Small-Angle Scattering. *Metall. Mater. Trans. A* **2010**, *41*, 1151−1158.
(27) Stolwijk, N. A.; Wiencierz, M.; Heddier, C.; Kösters, J. What Can We Learn from Ionic Conductivity Measurements in Polymer Electrolytes? A Case Study on Poly(ethylene Oxide) (PEO)-NaI and PEO-LiTFSI. *J. Phys. Chem. B* **2012**, *116*, 3065−3074.
(28) Chintapalli, M.; Le, T. N. P.; Venkatesan, N. R.; Mackay, N. G.; Rojas, A. A.; Thelen, J. L.; Chen, X. C.; Devaux, D.; Balsara, N. P. Structure and Ionic Conductivity of Polystyrene- *Block* -Poly(ethylene Oxide) Electrolytes in the High Salt Concentration Limit. *Macromolecules* **2016**, *49*, 1770−1780.
(29) Vincent, C. A. Ion Transport in Polymer Electrolytes. *Electrochim. Acta* **1995**, *40*, 2035−2040.
(30) Shterenberg, I.; Salama, M.; Yoo, H. D.; Gofer, Y.; Park, J.-B.; Sun, Y.-K.; Aurbach, D. Evaluation of $(CF_3SO_2)_2$ N^- (TFSI) Based Electrolyte Solutions for Mg Batteries. *J. Electrochem. Soc.* **2015**, *162*, 7118−7128.
(31) Dou, S.; Zhang, S.; Klein, R. J.; Runt, J.; Colby, R. H. Synthesis and Characterization of Poly(ethylene Glycol)-Based Single-Ion Conductors. *Chem. Mater.* **2006**, *18*, 4288−4295.
(32) Ha, S.-Y.; Lee, Y.-W.; Woo, S. W.; Koo, B.; Kim, J.-S.; Cho, J.; Lee, K. T.; Choi, N.-S. Magnesium(II) Bis(trifluoromethane Sulfonyl) Imide-Based Electrolytes with Wide Electrochemical Windows for Rechargeable Magnesium Batteries. *ACS Appl. Mater. Interfaces* **2014**, *6*, 4063−4073.
(33) Huq, R.; Farrington, G. Ion Transport in Divalent Cation Complexes of Poly (Ethylene Oxide). *Solid State Ionics* **1988**, *28−30*, 990−993.
(34) Yang, L. L.; McGhie, A. R.; Farrington, G. C. Ionic Conductivity in Complexes of Poly(ethylene Oxide) and $MgCl_2$. *J. Electrochem. Soc.* **1986**, *133*, 1380.
(35) Liebenow, C. A Novel Type of Magnesium Ion Conducting Polymer Electrolyte. *Electrochim. Acta* **1998**, *43*, 1253−1256.
(36) Lee, D. K.; Allcock, H. R. The Effects of Cations and Anions on the Ionic Conductivity of poly[bis(2-(2-Methoxyethoxy)ethoxy)-phosphazene] Doped with Lithium and Magnesium Salts of Trifluoromethanesulfonate and Bis(trifluoromethanesulfonyl)imidate. *Solid State Ionics* **2010**, *181*, 1721−1726.
(37) Wang, W.; Liu, W.; Tudryn, G. J.; Colby, R. H.; Winey, K. I. Multi-Length Scale Morphology of Poly(ethylene Oxide)-Based Sulfonate Ionomers with Alkali Cations at Room Temperature. *Macromolecules* **2010**, *43*, 4223−4229.
(38) Leibler, L. Theory of Microphase Separation in Block Copolymers. *Macromolecules* **1980**, *13*, 1602−1617.
(39) Mori, K.; Tanaka, H.; Hashimoto, T. Scattering Functions for Disordered Two-Component Polymer Systems Including Block Polymers. *Macromolecules* **1987**, *20*, 381−393.
(40) Mori, K.; Okawara, A.; Takeji, H. Order-Disorder Transition of Polystyrene-Block-Polyisoprene. I. Thermal Concentration Fluctuations in Single-Phase Melts and Solutions and Determination of χ as a Function of Molecular Weight and Composition. *J. Chem. Phys.* **1996**, *104*, 7765.
(41) Gunkel, I.; Thurn-Albrecht, T. Thermodynamic and Structural Changes in Ion-Containing Symmetric Diblock Copolymers: A Small-Angle X-Ray Scattering Study. *Macromolecules* **2012**, *45*, 283−291.

DOI: 10.1021/acs.macromol.6b01886
Macromolecules 2016, 49, 9139−9147